A simplified skyline-based method for estimating the annual solar energy potential in urban environments

Calcabrini, Andres; Ziar, Hesan; Isabella, Olindo; Zeman, Miro

DOI
10.1038/s41560-018-0318-6

Publication date
2019

Document Version
Final published version

Published in
Nature Energy

ARTICLES
https://doi.org/10.1038/s41560-018-0318-6
nature energy

A simplified skyline-based method for estimating the annual solar energy potential in urban environments

Andres Calcabrini*, Hesan Ziar, Olindo Isabella and Miro Zeman

Architects, engineers and urban planners have today at their disposal several tools for simulating the energy yield of photovoltaic systems. These tools are based on mathematical models that perform repetitive calculations to determine the annual irradiation received by solar panels; hence when photovoltaic systems are installed in complex urban environments, the simulations become highly computationally demanding. Here we present a simplified and yet accurate model for the direct calculation of the annual irradiation and energy yield of photovoltaic systems in urban environments. Our model is based on the correlation between the solar radiation components and the shape of the skyline profile. We show how calculations can be simplified by quantifying the skyline using two indicators: the sky view factor and the sun coverage factor. Model performance is evaluated in different climates using measured data from different photovoltaic systems. Results indicate that the proposed model significantly reduces the required computation time while preserving a high estimation accuracy.

The United Nations predicts that the global population is expected to reach 8.5 billion by 2030, and that by then most humans will be settled in densely populated cities[1]. Along with the growth of urban population, the International Energy Agency forecasts a major expansion of photovoltaic (PV) systems in urban areas: the residential PV market is expected to triple its size by 2030[2]. Moreover, different research studies[3,4] estimate that by using the available area on rooftops only in Europe and the United States the cumulative worldwide PV installed capacity could reach 2,000 GW. As such, PV systems in urban environments are of increasing relevance.

Aesthetically appealing and efficient PV modules are contributing to the rapid deployment and integration of PV systems in cities[5]. Besides the traditional building added photovoltaics (BAPV), today the PV market is offering more alternatives for building integrated photovoltaics (BIPV). Fairly soon, every surface will become a potential support for mounting PV modules; not only horizontal and tilted rooftops, but also vertical façades will allow the generation of affordable electricity from solar energy[6]. In this context, and aiming to find the best surfaces, it is evident there is a need for fast and accurate models to determine the solar energy potential in urban environments.

During recent decades, multiple software suites have been developed to compute the solar irradiation impinging on a surface and the energy yield of a PV system. Among these, we can find: In My Backyard tool[7], the PVSITES project[8], different ray-tracing-based simulation tools[9–11], various GIS-based methods[12,13] and many others[14]. The vast majority of these available tools calculate the hourly irradiance impinging on the plane of array (POA) considering the radiation intensity and distribution over the sky, the module tilt and orientation, and the objects surrounding the target surface[15]. By integrating hourly irradiance values over an entire year, the annual energy potential is obtained. For this reason, the previously mentioned methods are hereinafter referred to as irradiance-based approaches.

Irradiance-based approaches are needed when the power generated at every hour during a year is of interest. However, for some applications, only the annual energy potential is required. For instance, when looking at the optimum locations to install a distributed PV system in an urban planning framework, it is necessary to estimate the annual energy yield at a large number of locations. In this case, hourly irradiance levels are merely intermediate values that are needed to find the optimal locations. The repetitive calculation process combined with the complex geometry of the landscape make irradiance-based approaches highly computationally demanding[16,17].

In an effort to simplify the calculations and minimize the computation time, different methodologies and indicators for the solar potential in urban environments have been explored. For example, the work of Robinson shows that the sky view factor can be used as an irradiation indicator, particularly in locations with a high amount of diffuse radiation[18]. Rodriguez et al. presented an urban modelling platform[19] for estimating the solar potential using the three-dimensional (3D) geometry of buildings and the simple Hay and Davies sky model to reduce the computation time[20]. More recently, Chatzipoulka et al. presented a study in which the sky view factor is used as a predictor of the solar potential of vertical façades, allowing the quick estimation of the PV potential of building in latitudes between 38° and 60°[21]. These mentioned approaches are useful to give a quick estimation of the solar potential available in urban environments. Nevertheless, none of these methods has been validated using actual measured data.

Here, we present an alternative model for the direct estimation of the solar energy potential in urban areas. The proposed model can give accurate estimations of the annual irradiation impinging on a surface with a substantial reduction in the required computational power. We show that calculations can be accelerated by quantifying the urban landscape using two indicators: the sky view factor (SVF) and the sun coverage factor (SCF). Moreover, the model can also be adapted to estimate the energy yield of a PV system. The performance

Photovoltaic Materials and Devices Group, Electrical Sustainable Energy Department, Delft University of Technology, Delft, The Netherlands.
*e-mail: a.calcabrini-1@tudelft.nl

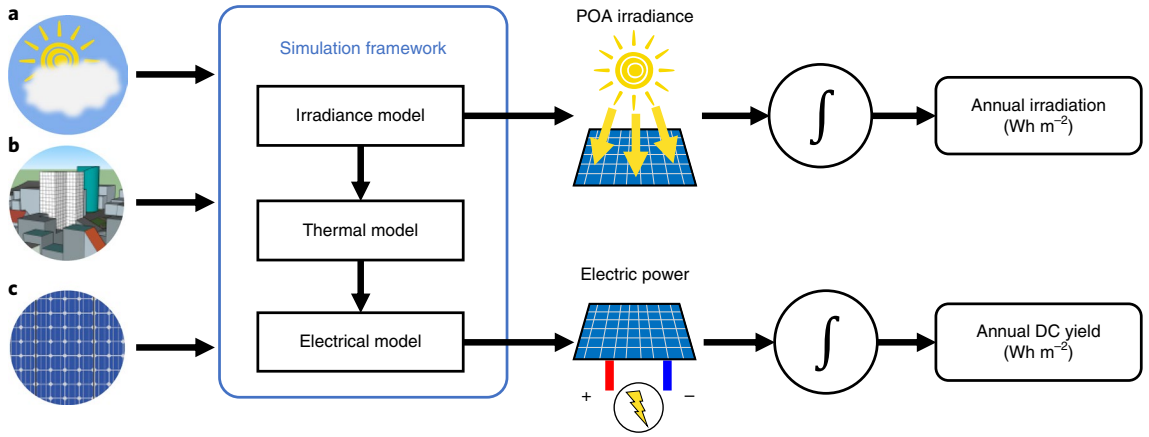

Fig. 1 | Irradiance-based approach. General block diagram of the simulation framework of irradiance-based approaches for calculating the annual irradiation on a surface and the PV system's annual DC yield. The required inputs are clustered into three groups. **a**, Meteorological data (that is, irradiance measurements, ambient and ground temperature, wind speed and cloud cover). **b**, Location specifications, including geographical coordinates and a 3D model of the landscape and objects surrounding the PV module. **c**, PV module data, which include mechanical, dimensional, electrical, optical and thermal parameters of the PV module. The irradiance model uses the location specifications and the meteorological data to calculate the amount of solar irradiance impinging on the POA of the PV module. The thermal model allows determination of the operating temperature of the PV module which, together with the computed irradiance, are the inputs to the electrical model to calculate the instantaneous power generated by the PV module.

and the deviations of the proposed method are hereby evaluated in different climates using real-time monitored PV systems.

The irradiance-based approach

Most irradiance-based approaches for calculating the annual irradiation and energy yield of a PV module combine irradiance, thermal and electrical models. These models constitute a simulation framework, as depicted in Fig. 1, which allows the calculation of the instantaneous irradiance on the POA and the electric power generated by the PV module.

Irradiance models generally comprise a decomposition and a transposition model. The decomposition model is used to generate direct normal irradiance (DNI) and diffuse horizontal irradiance (DHI) values from global horizontal irradiance (GHI) measurements. The transposition model combines the DNI and DHI values to determine the global POA irradiance[22]. Almost all transposition models calculate the total irradiance on the PV module (G_M^{tot}) by adding the contribution of three irradiance sources[23]:

$$G_M^{tot} = G_M^{dir} + G_M^{dif} + G_M^{alb} \quad (1)$$

where G_M^{dir} is the direct irradiance, which depends on the angle of incidence of the solar rays on the PV module and is proportional to the DNI, G_M^{dif} represents the sum of the diffuse circumsolar and the diffuse isotropic irradiance components of the simplified all-weather Perez irradiance model[24] and G_M^{alb} is the reflected irradiance, which is proportional to the surface albedo[25].

Applying equation (1), the total irradiance impinging on the PV module is calculated for every hour of the year. These values are then input to the thermal and electrical models to determine the generated electric power. Hourly results are integrated over an entire year to obtain the annual irradiation on the PV module and the generated DC electrical energy. Further details on the irradiance, thermal and electrical models used in this work are presented in the Methods section.

To avoid the repetitive calculations of the irradiance-based approaches, we propose using two indicators to directly estimate the annual irradiation. Hereby, we show how these indicators can be used to simplify the calculations and we give a mathematical expression for the proposed irradiation model. Furthermore, we give an example of how the model is applied to a specific PV system in urban environments, and we show how it can be extended to estimate the DC yield of PV systems.

Solar irradiation indicators

As shown in Fig. 1, the annual irradiation on a PV module depends on the local meteorological conditions. Since weather conditions are usually similar from one year to the next, we use climate data to estimate the average annual irradiation on a PV system. While weather data describe the atmospheric conditions for a particular year, climate data are obtained by evaluating weather conditions during several years (all the results presented in this work are obtained using climate data generated with METEONORM). From the outcome of the simulation using climate data, we have found that it is possible to describe the annual irradiation at a given location using two figures of merit that quantify the landscape surrounding a PV module.

The first indicator used to quantify the landscape around a PV module is the already mentioned SVF, which can be calculated from the skyline profile[26]. The SVF of a surface is a geometrical parameter defined as the fraction of radiant flux leaving the surface of the PV module which is intercepted by the sky[27]—that is, it represents the proportion of the sky that is visible from the central point of the PV module. This parameter is used because the aforementioned diffuse isotropic and ground reflected components of the Perez model depend (almost) linearly on the SVF[24].

However, the other irradiance components are not directly related to the SVF. In fact, it is easy to imagine a case where the direct and circumsolar irradiation components cannot be estimated using the SVF[18]. For example, for a horizontal solar panel in the Northern Hemisphere, none of the objects located on the north side of the PV module overlap with the sun path. These objects reduce the SVF but they affect neither the direct nor the diffuse circumsolar irradiance components which originate from the centre of the sun disk[28]. Therefore, to estimate the irradiation due to these other two components, we introduce a new indicator: the sun coverage factor, SCF. The SCF at a location with a raised horizon is defined as the ratio between time that the sun is behind the module or blocked by the skyline per year and the annual sunshine duration at the same location with a clear horizon.

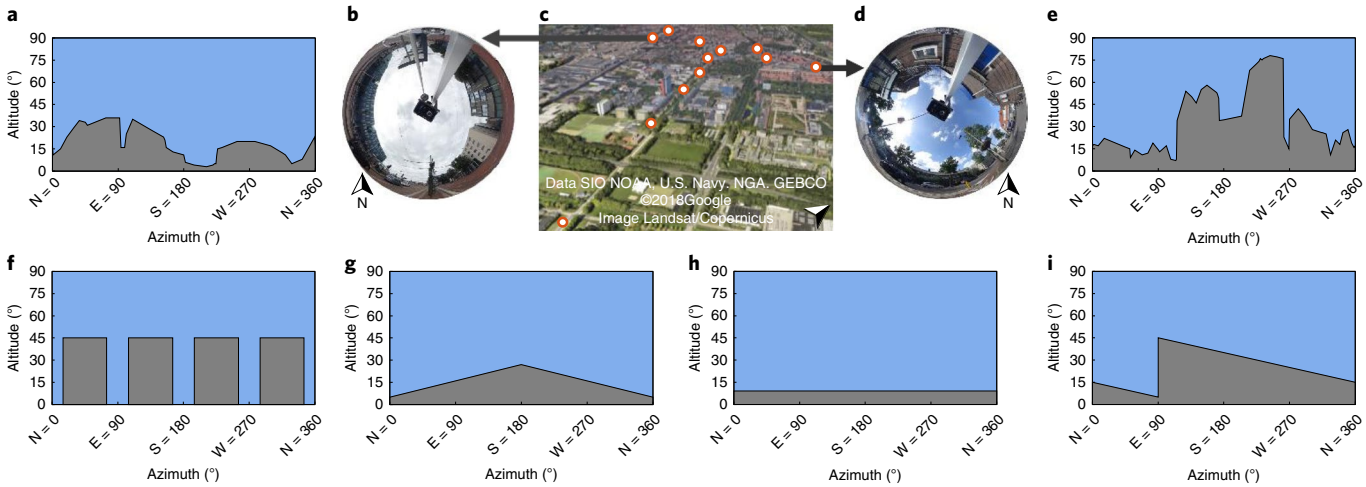

Fig. 2 | Synthetic and real skyline profiles. a–**e**, Real skylines for the city of Delft, the Netherlands. **c**, Each of the 12 spots in Delft where the real skyline profiles were captured. **b**,**d**, Examples of the images obtained with the Horicatcher tool at two different locations. **a**,**e**, Real skyline profiles obtained after the processing of the Horicatcher images. **f**–**i**, Synthetic skyline profiles. These synthetic skylines respectively correspond to the functions a_{spD5}, a_{spO4}, a_{spA1} and a_{spF5} listed in Supplementary Table 2.

It is evident that the SCF is not an irradiance-weighted parameter—that is, blocking the sun one hour in the morning and blocking the sun one hour at midday contribute in the same amount to reduce the SCF value. In some cases, this might result in a weak correlation with the hourly irradiation. However, the important advantage of using the SCF as an indicator is that it can be quickly determined by combining the skyline profile (which is already needed to determine the SVF) and the sun path[29].

Skyline profiles

A detailed 3D model of the environment surrounding the PV modules is required to precisely calculate the yield of a PV system. However, many irradiance-based approaches simply use the skyline profile at the system's location to compute the irradiation on the solar panels. The skyline profile is a 2D projection of the 3D surrounding landscape calculated at the central point of a PV module, and hence it is a simplification of the problem geometry that introduces errors in the calculations. Nevertheless, as explained in Supplementary Note 1, these deviations are considered acceptable.

Simulations have been carried out using a set of 161 synthetic skyline profiles to find the correlation between the above-mentioned indicators and the annual irradiation. Each synthetic profile consists of a number of geometrical shapes distributed along the horizon (see Supplementary Table 2). The advantage of using synthetic skylines lies in the fact the skyline shapes can be modified at will so as to mimic a wide range of different real urban landscapes. Figure 2 shows some examples of the synthetic profiles used to obtain the results presented in the following sections.

In addition, the skyline in 12 real locations in Delft were captured using the Horicatcher tool[30]. These real skyline profiles were used in the simulations to ensure that the synthetic skyline profiles are representative of actual urban landscapes. Figure 2 shows the points where the skylines were captured in Delft and the result of extracting the skyline from the Horicatcher pictures.

Simplified irradiation model

We have simulated the irradiance on tilted surfaces for each synthetic and real skyline profile to show how the annual irradiation components correlate with SVF and SCF. As an example, here we show the correlations found for the PV-powered e-Bike charging station (see Fig. 3a) for the case when its PV modules are tilted 51° and facing southwest.

In Fig. 3b, the sum of the simulated isotropic diffuse and albedo components (I_Y^{SVF}) is plotted against the SVF of the corresponding skyline profiles. For the above-mentioned reasons, there is a strong linear correlation between the variables. Deviations from the linear fit are due to the albedo component, since part of direct light impinging on the reflective surfaces is also reflected back on the PV modules. Moreover, the maximum SVF value on the horizontal axis equals 0.81 and it is the SVF of a module tilted 51° in a free horizon location.

In Fig. 3c, the sum of the simulated direct and circumsolar components (I_Y^{SCF}) is correlated with the SCF. From the minimum value in the horizontal axis, it can be noticed that since the PV modules are facing southwest and tilted 51°, even when the horizon is free, the sun is behind the POA 19% of the time. Besides, it can be observed that the drop in the annual irradiation is flatter for low SCF values and it becomes steeper as SCF increases. This can be explained by realizing that small SCF values usually correspond to low skyline profiles that block the sun mostly during sunrise and/or sunset, when the POA irradiance is much lower than at midday.

By adding the polynomial regressions in Fig. 3, the annual irradiation on a surface (I_Y) can be expressed as

$$I_Y = I_Y^{SCF} + I_Y^{SVF} \quad (2)$$

with

$$I_Y^{SCF} = \sum_{k=1}^{3} c_k (1 - SCF^k) \quad (3)$$

$$I_Y^{SVF} = (c_4 + c_5 \alpha_{gnd}) SVF \quad (4)$$

The coefficients $c_1, \ldots, c_5$ are obtained from the linear and cubic fittings shown in Fig. 3 and are valid for a specific module tilt and orientation within a geographical region with the same climate. Furthermore, the proposed irradiation model is independent of

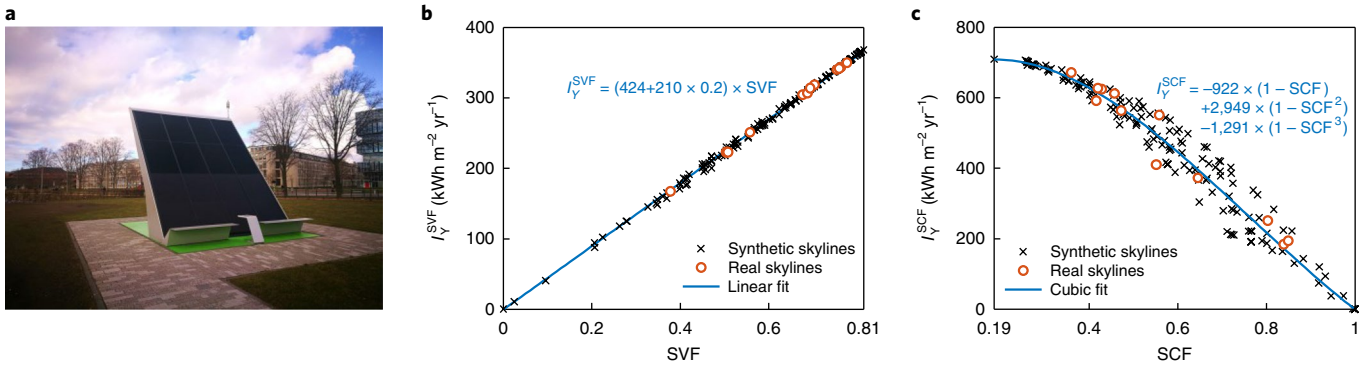

Fig. 3 | Model fitting to an actual PV system. Example of the correlation between SVF, SCF and the irradiation components for the southwest-facing e-Bike charging station tilted 51° for different synthetic and real skylines in Delft, the Netherlands. **a**, Image of the e-Bike charging station, a PV system developed at TU Delft for charging electric bikes with solar power. **b**, Correlation between SVF and the diffuse isotropic plus albedo irradiation. Each black cross on the plots represents the simulated irradiation on the e-Bike charging station for a different synthetic skyline profile and each orange circle indicates the simulated yield under a real skyline profile. The solid blue line and the equation in the plot correspond to the linear regression that fits the results. The 0.2 factor in the equation corresponds to the albedo coefficient of the ground around the e-Bike charging station. **c**, Correlation between SCF and the direct plus diffuse circumsolar irradiation. The solid blue line and the equation in the plot correspond to the cubic regression that fits the results.

Table 1 | Correlation coefficients for a 51° tilted surface in Delft, the Netherlands

A_M (°)	c_1 (kWh m^{-2} yr^{-1})	c_2 (kWh m^{-2} yr^{-1})	c_3 (kWh m^{-2} yr^{-1})	c_4 (kWh m^{-2} yr^{-1})	c_5 (kWh m^{-2} yr^{-1})
N = 0	−1,147	1,875	−801	411	144
NE = 45	−6,353	9,105	−3,863	411	148
E = 90	−2,261	4,344	−1,903	411	174
SE = 135	−895	2,708	−1,174	411	202
S = 180	−665	2,553	−1,143	411	211
SW = 225	−883	2,687	−1,173	411	199
W = 270	−2,025	3,980	−1,747	411	174
NW = 315	−5,960	8,526	−3,613	411	145

The coefficients have been calculated for the eight main PV module orientations (A_M) and can be used to estimate the annual irradiation on the e-Bike charging station. Whereas coefficients $c_1 - c_3$ are used to estimate the direct and diffuse circumsolar irradiation, coefficient c_4 is used to estimate the diffuse isotropic irradiation and coefficient c_5 is used to estimate the ground reflected irradiation.

the ground albedo (α_{gnd}), which can be changed in equation (4) to match the local albedo.

It should be noticed that in the case when the sky view is completely obstructed (for example, with an opaque dome) the SVF is 0 and the SCF is 1. Under these conditions, the estimated annual irradiation is zero. On the other hand, when the horizon is free, for a horizontal surface the maximum irradiation is given by

$$I_{Y(max)} = \sum_{k=1}^{4} c_k \quad (5)$$

Table 1 presents the coefficients for estimating the annual irradiation on the e-Bike charging station for different module orientations in Delft. To explain the use of these coefficients, we can consider the case of a south-facing PV system tilted 51° in Delft with a free horizon. For such system, SCF is 0.115 and SVF equals 0.814. Considering that the albedo of the bricks around the PV system in Fig. 3a is 0.2, the coefficients corresponding to a south-oriented surface in Table 1 can be substituted in equations (3) and (4) to calculate the annual irradiation, which equals 1.16 MWh m^{-2}.

Simplified energy yield model

Given the annual irradiation on a certain PV system, the operative efficiency of the PV modules must be calculated to estimate the annual DC yield. Among other factors, the operative efficiency depends on the module temperature and the irradiance level, and is defined as the actual conversion efficiency from solar irradiance to electric power of a PV module in the field. Operative efficiencies are generally lower than standard test conditions (STC) efficiencies, since the module operating temperature is usually higher than 25 °C. Despite the fact that the ambient temperature and the solar irradiance levels, which affect the operative efficiency, vary substantially from month to month, the relative variations in the monthly performance ratios of a PV system are generally lower than 10%[31]. This suggests that the proposed irradiation model can be extended to estimate the annual DC energy yield E_Y of a PV module, resulting in

$$E_Y = E_Y^{SCF} + E_Y^{SVF} \quad (6)$$

where

$$E_Y^{SCF} = \sum_{k=1}^{3} d_k (1 - SCF^k) \quad (7)$$

$$E_Y^{SVF} = (d_4 + d_5 \alpha_{gnd}) SVF \quad (8)$$

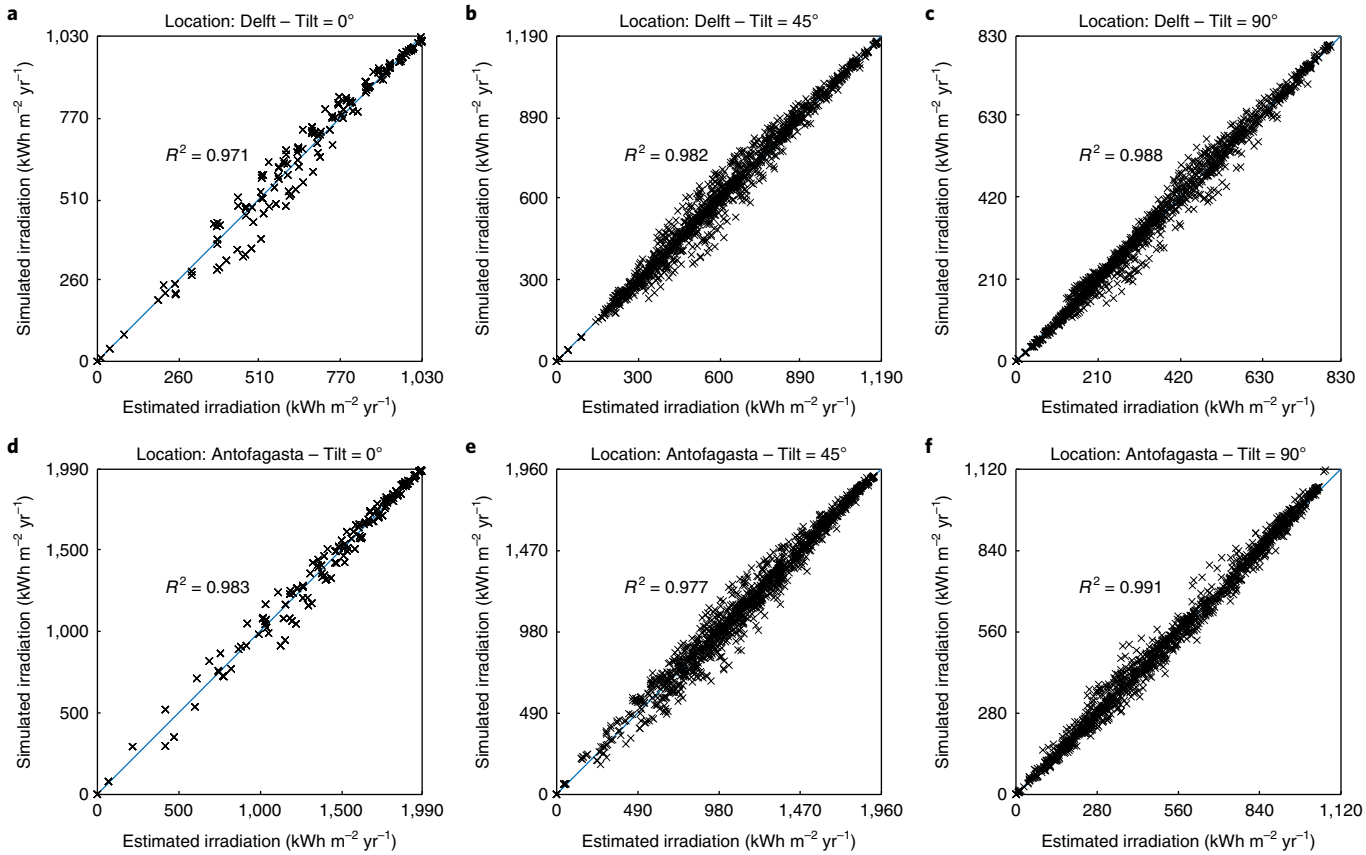

Fig. 4 | Model performance in sunny and cloudy climates. a–f, Benchmark study on the proposed annual irradiation model in Delft, the Netherlands (**a**–**c**) and Antofagasta, Chile (**d**–**f**) for different module tilt angles and orientations. Each black cross on the plot represents a study case in a different synthetic skyline profile. For each case studied, the annual irradiation was simulated using the irradiance-based (full) approach, represented by a value on the vertical axis, while the annual irradiation estimated with the proposed model is represented by a value on the horizontal axis. For surfaces tilted 45° and 90° (**b**, **c**, **e** and **f**), the comparison was carried with 161 synthetic skylines and 8 possible module orientations, amounting to 1,288 simulations. In the case of surfaces with 0° tilt (**a** and **d**), only 161 results are shown because the orientation of the surface is irrelevant when the surface is horizontal. Coefficients of determination R^2, which give an indication of the accuracy of the proposed model, are shown in the plots.

Table 2 | Model coefficients for estimating the DC yield of a JA Solar JAM6-60-270BK PV module tilted 35° in the southern part of the Netherlands

A_M (°)	d_1 (kWh yr^{-1})	d_2 (kWh yr^{-1})	d_3 (kWh yr^{-1})	d_4 (kWh yr^{-1})	d_5 (kWh yr^{-1})
N = 0	−249	467	−186	106	21
NE = 45	−536	964	−421	106	21
E = 90	−319	746	−315	106	23
SE = 135	−187	630	−262	106	25
S = 180	−160	648	−283	106	26
SW = 225	−193	648	−274	106	25
W = 270	−311	736	−314	106	23
NW = 315	−506	913	−397	106	21

The usefulness of a fast energy yield estimation model is self-evident. If we calculate the correlation coefficients for a specific PV system (for example, the e-Bike charging station), we can estimate how much electricity the system would generate in different sites in a city (see Supplementary Fig. 3). Then, it would be possible to use the digital elevation model of a urban area to create an energy potential map and find all the places where it is economically feasible to install a certain PV system.

Model benchmarking in different climates

The accuracy of the proposed annual irradiation model based on the SVF and SCF has been evaluated in different climates by comparing results with the full irradiance-based approach based on the Perez irradiance model. For this purpose, we first simulated the annual irradiation on surfaces with different tilt angles (0°, 45° and 90°) using the irradiance-based approach (that is, by integrating over an entire year the POA irradiance resulting

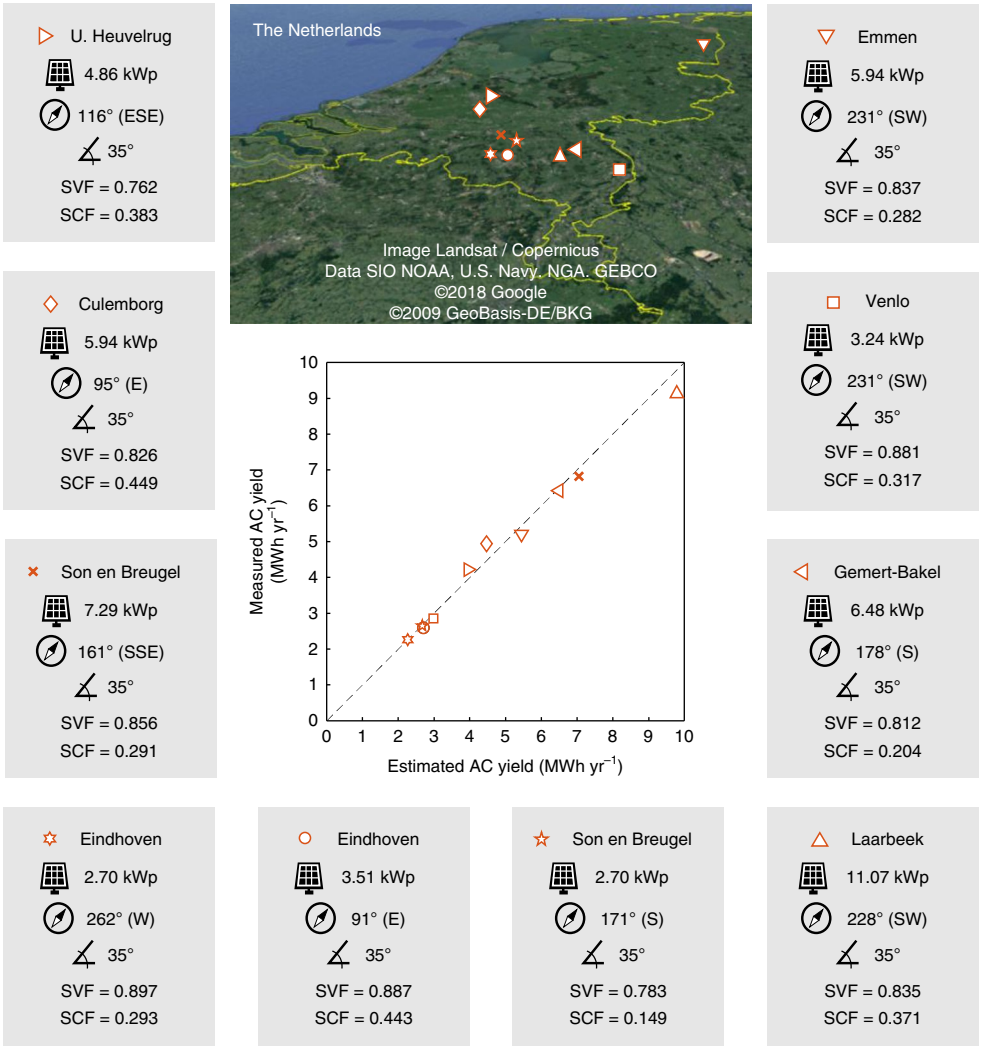

Fig. 5 | Model validation in the Netherlands. A set of ten PV systems installed and monitored in the Netherlands was evaluated for a one-year-long period between 2016 and 2017. The location of each of the systems is shown on the map. Each system is identified with a different marker. The location name, installed peak power, orientation, tilt angle and irradiation indicators for each system are presented in the grey boxes. All the systems studied have the same tilt (35°), type of PV modules (JA Solar JAM6-60-270BK) and inverter (SolarEdge SE3500). The comparison between the measured and estimated AC yields is shown in the central plot.

from equation (1)) in two cities with different climates: Delft, the Netherlands, where the mean annual horizontal global irradiation is approximately 1 MWh m^{-2} yr^{-1} and the mean annual cloud cover is 5.5 okta; and Antofagasta in the Atacama Desert, Chile, with 2 MWh m^{-2} yr^{-1} and 3.4 okta. Then, using the results of the irradiance-based approach, the regression coefficients c_1 to c_5 were generated (Supplementary Tables 3 and 4). Finally, the SVF and the SCF for each synthetic skyline profile were calculated to estimate the annual irradiation using the previously calculated correlation coefficients in equations (2)–(4).

The deviations between the annual irradiation estimated using the two indicators were compared with the annual irradiation obtained with the full irradiance-based simulation performed in the first instance. Figure 4 shows the correspondence between the results of the irradiance-based approach and our proposed model. The high values of the coefficient of determination ($R > 0.97$ for all cases) show a good overall performance of our model for both climates. Moreover, in 85% of the studied cases, the relative deviations between both methods are lower than 10%. Lastly, it is important to mention that the largest deviations are associated with surfaces with low solar energy potential, which are also the least attractive ones for mounting PV modules.

Validation study in the Dutch climate

The annual energy yield model has been applied to estimate the yield of multiple PV systems monitored in the Netherlands. Ten grid-connected PV systems with the same tilt ($\theta_M = 35°$), PV modules (JA Solar JAM6-60-270BK) and inverters (SolarEdge SE3500) have been studied. The coefficients of the annual DC yield model were calculated using climate data and the results were compared to the actual energy yield measured between 2016 and 2017.

The coefficients for estimating the annual DC yield of the PV modules are presented in Table 2. It is important to notice that these coefficients are valid only for a particular PV module model with a specific tilt angle. This limitation is a consequence of extending the irradiation model to calculate the DC energy yield.

For every PV system, the irradiance indicators (SVF and SCF) were calculated at the central point of the PV array using skylines profiles generated from a LIDAR digital elevation model[32]. With these values, the coefficients given in Table 2 and assuming

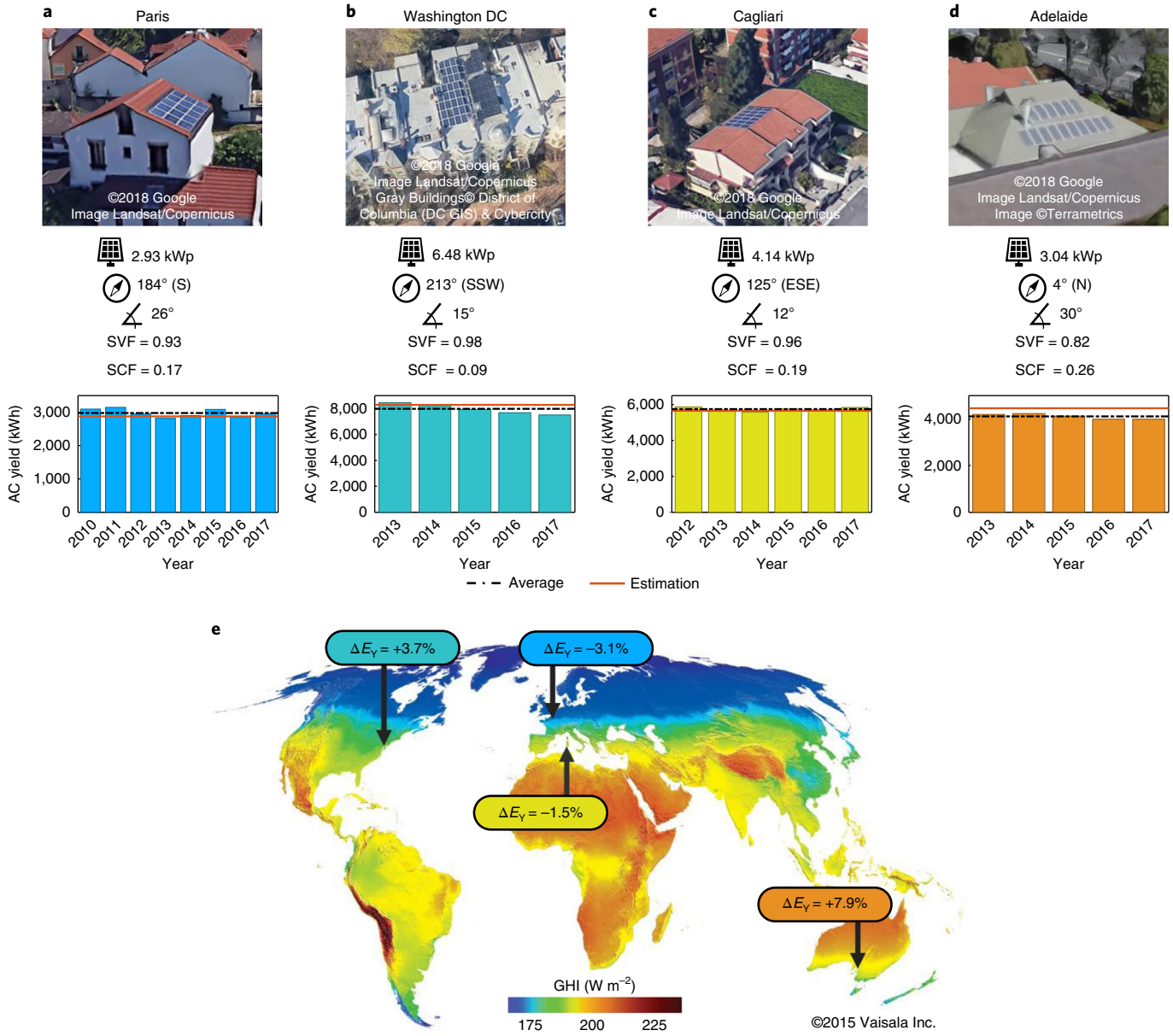

Fig. 6 | Model validation using four PV systems in different climates. a, Picture and characteristics of the PV system studied in Paris, France. The bar graph at the bottom shows the annual generated electricity measured by the inverter of the system between 2010 and 2017. The dashed line in the plots represents the average annual generation, and the red solid line indicates the production estimated by our proposed model. **b**, Picture and characteristics of the PV system studied in Washington DC, USA. The bar graph shows the AC yield measured between 2013 and 2017. **c**, Picture and characteristics of the PV system studied in Calgiari, Italy. The bar graph shows the AC yield measured between 2012 and 2017. **d**, Picture and characteristics of the PV system studied in Adelaide, Australia. The bar graph shows the AC yield measured between 2013 and 2017. **e**, Map of global horizontal irradiance. Credit: © 2015 Vaisala Inc. The arrows on the map indicate the locations of the four PV systems analysed from the online platform PVOutput[34]. The colour scale on the map shows the difference in the annual mean global horizontal irradiance (GHI) over the entire globe. ΔE_Y is the relative deviation between the average measured yield by each system and the estimation obtained with the proposed annual energy yield model.

an average albedo of 0.2, the annual DC yield of the systems can be calculated. However, as most PV systems measure only the AC generated electricity, it is necessary to estimate the AC yield of the PV systems from the DC yield of the PV modules. The ultimate AC yield has been calculated taking into account the European efficiency of the SE3500 solar inverter (97.6%) and the following system losses[33]: maximum power point tracking (MPPT) losses (accounting for 1% absolute efficiency loss at system level), module mismatch losses (1% absolute), Ohmic losses (3% absolute), availability of the system (1% absolute) and soiling losses (1% absolute). All factors taken into account, the resulting ultimate DC to AC conversion efficiency is 90.6%. In Fig. 5 the characteristics and performance of the analysed PV systems is presented. From the comparison between the measured and estimated AC yields, it is concluded that the average estimation error is 0.7%, while the maximum error corresponds to the PV system installed in Culemborg (underestimated by 9.8%). The energy yield of small PV systems (up to 5 kWp) is estimated with high accuracy (the largest deviation is 4% for the system in Venlo). On the other hand, the yield of large systems is slightly overestimated. This overestimation is most likely due to fact that the

sky view of PV modules in a large system can differ substantially (that is, one module can be much more shaded than another). To improve the estimation, the SVF and SCF values could be calculated at different points in the array.

Validation study in different climates

The model performance was also evaluated in different climates using PV systems from the PVOutput online database[34]. PVoutput is a free online service that allows its users to configure their PV systems to automatically upload live monitored data. We looked for systems in the database that fulfill the following six criteria: monitoring time must be longer than five years; data loss for any year must be lower than 1% (that is, three days per year); the generated electrical energy must be consistent through time; the PV system must be visible on Google Earth; photogrammetry data must be available to reconstruct the landscape; the PV module and inverter models must be identified.

Following the selection criteria, four PV systems were selected. The landscape surrounding each system was reconstructed using photogrammetry data (Supplementary Note 2). The correlation coefficients for each of these systems were obtained using climate data generated with METEONORM and the AC energy yield was determined as in the case of the systems in the Netherlands. Figure 6 again shows a good agreement between the estimations and the measurements. The largest deviation corresponds to the system in Adelaide (7.9%), but it should not be associated with the high irradiation level at this location. The AC yield bar graph corresponding to the system in Adelaide shows a decreasing trend in time. This drop is partly due to the meteorological conditions (the annual global irradiation in Adelaide has decreased approximately 4% from 2013 to 2017[35]), but it could also be associated with the degradation of PV module performance, which is not considered in the annual energy yield model.

Improvement in computation time

The model proposed in this paper implies a great improvement in terms of computational complexity. We compared the computation time of our method with that of the irradiance-based approach using implementations in MATLAB. On average, the simulation using the irradiance-based approach took 260 ± 30 ms, whereas using our simplified model it took only 14 ± 2 ms. Moreover, the amount of memory required by our model is more than a thousand times lower.

By combining our model with different methods for obtaining the skyline from 3D urban point clouds[36,37], it is possible to quickly generate a solar energy potential map. Considering the above-mentioned simulation times, the calculation of the potential of a PV system over a 100 m by 100 m cadastre with 1 m resolution using the irradiance-based approach would take 43 minutes, whereas our method could do it in only 2 minutes. Furthermore, the computation time can be substantially reduced using a graphics processing unit (GPU) to allow quick assessment of much larger areas.

The main advantage of our model is the introduction of the SCF to estimate the direct and circumsolar irradiation. The SCF can be rapidly calculated knowing the sun path and the shape of the skyline profile. Nevertheless, the SCF is not an irradiance-weighted parameter and our model presents higher deviations in the case of surfaces with a low solar potential; which, however, are the least interesting for PV applications.

The accuracy and speed achieved with the proposed model can be used to improve current solar-based urban planning design methods to take into account the solar potential of a building as a design parameter[38–40]. As an example, by applying our model, it would be possible to find the optimum shape and distribution of buildings in a cadastre to maximize the solar energy potential of the entire group of buildings.

Conclusions

This work reports on a simplified model to directly estimate the irradiation on a surface and the yield of a PV system in urban areas using two indicators: the SVF and the SCF. The proposed model requires the generation of five coefficients that depend on the local climate. These coefficients are generated one time, and later used to predict the irradiation and yield of a PV system at any place within a region with a similar climate. At this place, the SVF and the SCF of the PV module must be determined, and using the corresponding correlation coefficients the annual irradiation and yield can be quickly calculated.

The outcomes of the validation studies show that the maximum estimation error of the proposed model is lower than 10%. Moreover, our method entails a substantial reduction in the computational requirements for calculating the yield of PV systems in complex urban environments. This improvement allows one to quickly transform digital elevation models into detailed solar energy potential maps which can help architects, engineers and urban planners to build more sustainable cities.

Methods

The simulation framework. The transposition model used in this study distinguishes three irradiance components: direct, diffuse and reflected.

The direct beam component G_M^{dir} is proportional to the measured DNI[41] and can be expressed as

$$G_M^{dir} = \mathrm{DNI}\cos(\mathrm{AOI}) \tag{9}$$

where AOI is the angle between the solar vector and the normal to the PV module front surface[23].

The diffuse irradiance component G_M^{dif} is obtained from the measured DHI. For this study the simplified version of the anisotropic Perez model[28] was used, which divides the diffuse irradiance into three sub-components: isotropic (G_M^{iso}), circumsolar (G_M^{cir}) and horizontal ribbon (G_M^{hr}), each of them respectively corresponding to the terms in equation (10):

$$G_M^{dif} = \mathrm{DHI}\left[(1-F_1)\mathrm{SVF} + F_1\frac{a}{b} + F_2\sin(\theta_M)\right] \tag{10}$$

where F_1 and F_2 are empirical coefficients, respectively corresponding to the circumsolar and horizontal ribbon components, a and b are geometrical coefficients that depend on the sun position, and SVF is the sky view factor.

For a tilted module mounted close to the ground, the ground reflected component (also called the albedo component) is assumed to be proportional to the albedo coefficient of the ground surface α_{gnd}:

$$G_M^{alb} = \mathrm{GHI}\ \alpha_{gnd}\ (1-\mathrm{SVF}) \tag{11}$$

Following the calculation of the POA irradiance, the module temperature must be determined using a thermal model. In this study, the fluid dynamic model proposed in ref. [42] is used to estimate the temperature of the module in the steady state. The fluid dynamic model takes into account variables such as the wind speed, ambient and ground temperatures, the cloud cover, the mounting and the total plane of array irradiance.

The effective radiation reaching the solar cell and its temperature are the inputs to an electrical model that is used to determine the generated current and voltage. Despite it having been shown that the single and double diode models[43] are the most precise models for calculating the power output, here the model described in[44] has been used for it offers high accuracy and all the parameters that the model requires can be easily obtained from the PV module datasheet. The PV module efficiency η_M at given irradiance (G_M^{tot}) and temperature (T_M) levels is given by

$$\eta_M = \eta_M^{STC}[1+\beta(T_M - T_M^{STC})]\left[1+\ln\left(\frac{G_M^{tot}}{G_M^{STC}}\right)^{\gamma}\right] \tag{12}$$

where η_M^{STC} is the efficiency of the module under STC, β is module's power temperature coefficient and γ is given by

$$\gamma = \frac{N_s n k_B T_M}{q V_{OC}^{STC}} \tag{13}$$

where N_s is the number of series-connected PV cells in the module, n the ideality factor of the solar cell, which depends on the PV technology[45], k_B the Boltzmann

constant, q the elementary charge and V_{OC}^{STC} the open-circuit voltage of the module under STC.

The effect of the skyline on the solar irradiance components. The calculation of the irradiance components in raised horizon locations is modified according to the following assumptions:

- G_M^{dir}: the direct component is concentrated in the sun disk, yet in the simplified Perez model the sun is assumed to be a point source centred in the sun disk[24]. Therefore, this component is null when the sun is blocked by the skyline profile.
- G_M^{cir}: the circumsolar radiation is distributed around the sun disk, but in the Perez model it is also reduced to a point source centred at the sun disk. Consequently, this component is also null when the sun is blocked.
- G_M^{hr}: when the objects that constitute the skyline profile are low and very distant from the module, the horizontal ribbon component is only slightly affected. However, if the objects are close to the POA, as in most urban landscapes, the contribution of the horizontal ribbon is considered negligible[46].
- G_M^{iso}: the diffuse isotropic radiation is reduced proportionally to the SVF.
- G_M^{alb}: the reflected radiation is proportional to the global horizontal radiation which in turn depends on the skyline profile (SP). If the skyline is above the horizon line, the global horizontal radiation reaching the ground surface is equal to GHI_{sp}, which depends on the position of the sun:
- $GHI_{SP} = DNI\ \sin(a_S) + DHI\left[(1-F_1)\ SVF + F_1\frac{a}{b}\right]$, if the sun is in front of the module and above the skyline.
- $GHI_{SP} = DHI\ (1-F_1)\ SVF$, if the sun is behind the module or blocked by the skyline profile.

Calculation of the SVF. The SVF at a free horizon location (SVF_{fh}) is a function of only module tilt (θ_M) and can be expressed as

$$SVF_{fh}(\theta_M) = \frac{1+\cos(\theta_M)}{2} \tag{14}$$

However, in locations with a raised horizon the SVF must be calculated by numerical integration. This can be done using the work of Steyn for fisheye-lens pictures of the skyline[26]. Steyn divides the images of the skyline into multiple slices and rings that define a number circular sectors to calculate the SVF (Supplementary Fig. 4). Each of the circular sectors is mapped into rectangular sectors when the skyline is projected onto a Cartesian altitude-versus-azimuth plot like the ones shown in Fig. 2. Steyn gives the analytic expression to calculate the contribution of each of these sectors to the SVF value. Given an arbitrary skyline, the SVF can be computed by adding the weight of the sectors corresponding to visible parts of the sky.

When a PV module is tilted in a raised horizon location, the light coming from the part of the sky that lies behind the plane of array cannot reach the front surface (Supplementary Fig. 5). This part of the sky blocked by the POA also contributes to reduce the SVF, thus it must be added to the skyline profile (Supplementary Fig. 6). It can be shown, that a rectangular sky sector in the altitude-versus-azimuth plot centred at a point with azimuth A_P and elevation a_P is behind the POA of a PV module with azimuth A_M and tilt θ_M if the following conditions are met simultaneously

$$|A_P - A_M| < \frac{\pi}{2} \tag{15}$$

$$\cos(a_P) < (1+(\tan(\theta_M)\cos(A_P-A_M))^2)^{-\frac{1}{2}} \tag{16}$$

These two conditions allow one to identify the sky sectors blocked by the POA, and Steyn's method can be used to calculate the reduction in the SVF value. It can also be demonstrated that this method of calculating the SVF converges to equation (14) at free horizon locations.

Mathematical definition of the SCF. In locations with a raised horizon, such as urban environments, the altitude of the skyline profile (a_{sp}) can be described as a function of the azimuth (A):

$$a_{sp}(A), A \in [0^\circ, 360^\circ) \tag{17}$$

Using the previous definition, the SCF can be mathematically expressed as

$$SCF = \frac{\int_{year} \chi_{sp}(A_S(t), a_S(t))\,dt}{\int_{year} \chi_{fh}(a_S(t))\,dt} \tag{18}$$

where A_S and a_S are the solar azimuth and elevation respectively and

$$\chi_{sp}(A_S, a_S) = \begin{Bmatrix} 1 & 0 < a_S \le a_{sp}(A_S) \\ 0 & \text{otherwise} \end{Bmatrix} \tag{19}$$

$$\chi_{fh}(a_S) = \begin{Bmatrix} 1 & a_S > 0 \\ 0 & \text{otherwise} \end{Bmatrix} \tag{20}$$

Data availability

The data that support the plots within this paper and other findings of this study are available from the corresponding authors upon reasonable request.

Received: 19 June 2018; Accepted: 18 December 2018;
Published online: 4 February 2019

References

1. *World Urbanization Prospects: The 2014 Revision* (United Nations Department of Economics and Social Affairs, Population Division, 2015).
2. Frankl, P., Nowak, S., Gutschner, M., Gnos, S. & Rinke, T. *Technology Roadmap: Solar Photovoltaic Energy* (International Energy Association, 2010).
3. Huld, T. et al. The Rooftop Potential for PV Systems in the European Union to deliver the Paris Agreement. *European Energy Innovation* **Spring 2018**, 12–15 (2018).
4. Gagnon, P., Margolis, R., Melius, J., Phillips, C. & Elmore, R. *Rooftop Solar Photovoltaic Technical Potential in the United States. A Detailed Assessment* Technical Report NREL/TP-6A20-65298 (National Renewable Energy Lab, 2016).
5. Ballif, C., Perret-Aebi, L.-E., Lufkin, S. & Rey, E. Integrated thinking for photovoltaics in buildings. *Nat. Energy* **3**, 438–442 (2018).
6. Redweik, P., Catita, C. & Brito, M. Solar energy potential on roofs and facades in an urban landscape. *Sol. Energy* **97**, 332–341 (2013).
7. Anderson, K. H., Coddington, M. H. & Kroposki, B. D. Assessing technical potential for city PV deployment using NREL's In My Backyard tool. In *IEEE 35th Photovoltaic Specialists Conference (PVSC)* 001 085–001 090 (IEEE, 2010); https://doi.org/10.1109/PVSC.2010.5614697
8. Espeche, J. M., Noris, F., Lennard, Z., Challet, S. & Machado, M. PVSITES: building-integrated photovoltaic technologies and systems for large-scale market deployment. *Proceedings* **1**, 690 (2017).
9. Compagnon, R. Solar and daylight availability in the urban fabric. *Energy Build.* **36**, 321–328 (2004).
10. Lagios, K., Niemasz, J. & Reinhart, C. F. Animated building performance simulation (ABPS)-linking Rhinoceros/Grasshopper with Radiance/Daysim. In *4th National Conference of IBPSA-USA SimBuild 2010* 321–327 (IBPSA-USA, 2010).
11. Kämpf, J. H., Montavon, M., Bunyesc, J., Bolliger, R. & Robinson, D. Optimisation of buildings' solar irradiation availability. *Sol. Energy* **84**, 596–603 (2010).
12. Brito, M. C., Gomes, N., Santos, T. & Tenedório, J. A. Photovoltaic potential in a Lisbon suburb using lidar data. *Sol. Energy* **86**, 283–288 (2012).
13. Agugiaro, G. et al. Solar radiation estimation on building roofs and web-based solar cadastre. *ISPRS Ann. Photogram. Remote Sens. Spatial Inf. Sci.* **I-2**, 177–182 (2012).
14. Freitas, S., Catita, C., Redweik, P. & Brito, M. C. Modelling solar potential in the urban environment: state-of-the-art review. *Renew. Sustain. Energy Rev.* **41**, 915–931 (2015).
15. Lindberg, F., Jonsson, P., Honjo, T. & Wästberg, D. Solar energy on building envelopes—3D modelling in a 2D environment. *Solar Energy* **115**, 369–378 (2015).
16. Carneiro, C. et al. Urban environment quality indicators: application to solar radiation and morphological analysis on built area. In *Proc. 3rd WSEAS International Conference on Visualization, Imaging and Simulation* 141–148 (WSEAS, 2010).
17. Jakubiec, J. A. & Reinhart, C. F. Towards validated urban photovoltaic potential and solar radiation maps based on LiDAR measurements, GIS data, and hourly DAYSIM simulations. In *Proc. 5th National Conference of IBPSA-USA SimBuild 2012* 628–637 (IBPSA, 2012).
18. Robinson, D. Urban morphology and indicators of radiation availability. *Sol. Energy* **80**, 1643–1648 (2006).
19. Rodrguez, L. R., Duminil, E., Ramos, J. S. & Eicker, U. Assessment of the photovoltaic potential at urban level based on 3d city models: A case study and new methodological approach. *Sol. Energy* **146**, 264–275 (2017).
20. Davies, J. & Hay, J. Calculation of the solar radiation incident on an inclined surface. In *Proc. First Canadian Solar Radiation Data Workshop* 59–72 (Supply and Services Canada, 1978).

21. Chatzipoulka, C., Compagnon, R., Kaempf, J. & Nikolopoulou, M. Sky view factor as predictor of solar availability on building façades. *Sol. Energy* **170**, 1026–1038 (2018).
22. Reindl, D., Beckman, W. & Duffie, J. Evaluation of hourly tilted surface radiation models. *Sol. Energy* **45**, 9–17 (1990).
23. Smets, A. H. et al. *Solar Energy: The Physics and Engineering of Photovoltaic Conversion Technologies and Systems*. (UIT Cambridge, Cambridge, 2016).
24. Perez, R., Seals, R., Ineichen, P., Stewart, R. & Menicucci, D. A new simplified version of the Perez diffuse irradiance model for tilted surfaces. *Sol. Energy* **39**, 221–231 (1987).
25. Ineichen, P., Perez, R. & Seals, R. The importance of correct albedo determination for adequately modeling energy received by tilted surfaces. *Sol. Energy* **39**, 301–305 (1987).
26. Steyn, D. The calculation of view factors from fisheye-lens photographs: research note. *Atmos. Ocean* **18**, 254–258 (1980).
27. Johnson, G. T. & Watson, I. D. The determination of view-factors in urban canyons. *J. Clim. Appl. Meteorol.* **23**, 329–335 (1984).
28. Perez, R., Ineichen, P., Seals, R., Michalsky, J. & Stewart, R. Modeling daylight availability and irradiance components from direct and global irradiance. *Sol. Energy* **44**, 271–289 (1990).
29. Blanco-Muriel, M., Alarcón-Padilla, D. C., López-Moratalla, T. & Lara-Coira, M. Computing the solar vector. *Solar Energy* **70**, 431–441 (2001).
30. *Meteonorm Handbook Part I: Software* version 7.2 (Meteotest, Bern, 2017).
31. Carr, A. & Pryor, T. A comparison of the performance of different PV module types in temperate climates. *Sol. Energy* **76**, 285–294 (2004).
32. *Actueel Hoogtebestand Nederland* (AHN, accessed 2 May 2018); http://www.ahn.nl/common-nlm/contactahn.html
33. Marion, B., et al. Performance parameters for grid-connected PV systems. In *Conference Record of the 31st IEEE Photovoltaic Specialists Conference* 1601–1606 (IEEE, 2005); https://doi.org/10.1109/PVSC.2005.1488451.
34. *PVOutput* (PVOutput, 2013); http://www.pvoutput.org/
35. *Monthly Mean Daily Global Solar Exposure* (Australian Government Bureau of Meteorology, accessed 7 October 2018); http://www.bom.gov.au/jsp/ncc/cdio/weatherData/av?p_nccObsCode=203&p_display_type=dataFile&p_startYear=&p_c=&p_stn_num=023119
36. Gál, T., Lindberg, F. & Unger, J. Computing continuous sky view factors using 3d urban raster and vector databases: comparison and application to urban climate. *Theor. Appl. Climatol.* **95**, 111–123 (2009).
37. An, S. et al. Three-dimensional point cloud based sky view factor analysis in complex urban settings. *Int. J. Climatol.* **34**, 2685–2701 (2014).
38. Kanters, J. & Horvat, M. Solar energy as a design parameter in urban planning. *Energy Procedia* **30**, 1143–1152 (2012).
39. Amado, M. & Poggi, F. Solar urban planning: a parametric approach. *Energy Procedia* **48**, 1539–1548 (2014).
40. De Luca, F. Solar form finding. subtractive solar envelope and integrated solar collection computational method for high-rise buildings in urban environments. In *Proc. 37th Annual Conference of the Association for Computer Aided Design in Architechture* (eds Nagakura, T. et al.) 212–221 (2017).
41. Demain, C., Journée, M. & Bertrand, C. Evaluation of different models to estimate the global solar radiation on inclined surfaces. *Renew. Energy* **50**, 710–721 (2013).
42. Fuentes, M. K. *A Simplified Thermal Model for Flat-plate Photovoltaic Arrays* Technical Report SAND85-0330-UC-63, 5 (Sandia National Labs, 1987).
43. Xiao, W., Dunford, W. G. & Capel, A. A novel modeling method for photovoltaic cells. In *IEEE 35th Annual Power Electronics Specialists Conference (PESC 04)* Vol. 3, 1950–1956 (IEEE, 2004); https://doi.org/10.1109/PESC.2004.1355416.
44. Lasnier, F. & Ang, T. G. *Photovoltaic Engineering Handbook* (Adam Hilger, New York, 1990).
45. Jain, A. & Kapoor, A. A new method to determine the diode ideality factor of real solar cell using Lambert w-function. *Sol. Energy Mater. Sol. Cells* **85**, 391–396 (2005).
46. *Meteonorm Handbook Part II: Theory* version 7.2 (Meteotest, Bern, 2017).

Acknowledgements

We thank the Dutch company Solar Monkey (www.solarmonkey.nl) for providing skyline profiles and annual AC yield measurements of PV systems monitored in the Netherlands for the validation of our model.

Author contributions

A.C., O.I. and M.Z. conceived the research. A.C. worked on modelling and the validation analysis. H.Z. and O.I. helped with the analysis and validations. O.I. and M.Z. supervised the whole project. All authors discussed the results and contributed to the writing of the paper.

Competing interests

The authors declare no competing interests.

Additional information

Supplementary information is available for this paper at https://doi.org/10.1038/s41560-018-0318-6.

Reprints and permissions information is available at www.nature.com/reprints.

Correspondence and requests for materials should be addressed to A.C.

Publisher's note: Springer Nature remains neutral with regard to jurisdictional claims in published maps and institutional affiliations.